JOURNAL OF MATERIALS SCIENCE 21 (1986) 895–903

# Effect of the filament nature on fatigue crack growth in titanium based composites reinforced by boron, B($B_4C$) and SiC filaments

P. SOUMELIDIS, J. M. QUENISSET, R. NASLAIN
*Laboratoire de Chimie du Solide du CNRS, Université de Bordeaux-I, 351 Cours de la Libération, 33405 Talence Cedex, France*

N. S. STOLOFF
*Materials Engineering Department, Rensselaer Polytechnic Institute, Troy, New York 12180, USA*

Crack propagation testing has been applied to synthetic metal matrix composites (MMC) in order to compare failure mechanisms in Ti–6Al–4V alloy reinforced by uncoated boron, B($B_4C$) and chemical vapour deposition (CVD) SiC filaments. The impeding effect of the fibres leads to low crack growth rates, compared to those reported for the unreinforced Ti–6Al–4V alloy and to higher toughness despite the presence of the reinforcing brittle phases. After long isothermal exposures at 850° C, the MMC crack growth resistance is reduced mainly due to fibre degradation, fibre–matrix debonding and an increase in matrix brittleness. However, for short-time isothermal exposures (up to about 10 h for B/Ti–6Al–4V, 30 h for B($B_4C$)/Ti–6Al–4V and 60 h for SiC/Ti–6Al–4V) the crack growth resistance is significantly increased. This improvement is related to the build up of an energy-dissipating mechanism by fibre microcracking in the vicinity of the crack tip. This damaging mechanism allowing matrix plastic deformation is already effective for boron and B($B_4C$) in the as-fabricated state, but occurs only after 10 h of thermal exposure at 850° C in the case of SiC/Ti–6Al–4V composites.

## 1. Introduction

Synthetic metal matrix composites (MMC) are often very sensitive to high temperature exposures since they are non-equilibrium thermodynamic systems. In order to extend MMC usefulness for high temperature structural applications and therefore to control fibre–matrix (FM) chemical reactions, various kinds of multiphase reinforcing filaments have been proposed (e.g. boron, Borsic, B($B_4C$), SiC filaments). These large diameter fibres ($\approx 140\,\mu m$) obtained by chemical vapour deposition on a tungsten or carbon core, have improved MMC behaviour in different ways depending on the filament nature (tensile strength, FM chemical compatibility, impact resistance, thermal fatigue resistance etc.).

Different studies have extensively depicted, in such synthetic composites, the chemical features of the FM interfacial reaction zone, after isothermal exposures. Furthermore, correlations between MMC mechanical behaviour and the reaction zone thickness have been proposed by several authors (many references are given in [1]). However, almost no work on MMC deals simultaneously with filament nature, isothermal exposure and crack growth mechanisms.

The aim of the present contribution is to compare titanium alloy matrix composites reinforced by either uncoated boron, B($B_4C$) or SiC filaments, from failure mechanism and toughness standpoints, for various thermal treatments. The method used for investigating crack propagation has been previously described [1].

The great differences existing between the conditions required to apply linear elastic fracture mechanics (LEFM) to rupture of materials and the conditions corresponding to MMC failure leads to uncertainties, especially in toughness determination. Nevertheless LEFM applied to fatigue crack propagation in MMC notched specimens gives sufficient indications about the different features of MMC mechanical behaviour (crack growth rate, rupture energy) for a better understanding of the effects of both filament nature and isothermal exposure.

TABLE I Mechanical characteristics of the brittle phases appearing at FM interfaces in titanium based composites reinforced with boron, B($B_4C$) or SiC filaments [4–8]

| | B | $B_4C$ | SiC | TiC | $TiB_2$ | $Ti_5Si_3$ |
|---|---|---|---|---|---|---|
| Young's modulus $E$ (GPa) | 440 | 490 | 450 | 440 | 540 | 235 |
| Rupture stress $\sigma^R$ (MPa) | 3500 | 2800 | 4100 | 1250 | 1350 | 1560 |
| Rupture strain $\varepsilon^R$ ($10^{-3}$) | 8 | 5.7 | 9.1 | 2.8 | 2.5 | 6.6 |

0022–2461/86 $03.00 + .12 

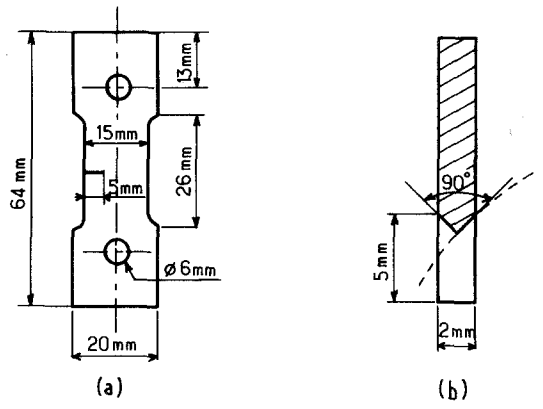


*Figure 1* (a) Specimen shape and size, (b) chevron notch.

## 2. Experimental details

Experimental conditions related to the sample synthesis, heat treatment and crack propagation testing have been previously detailed [1]; only their main features will be recalled here.

### 2.1. Materials

The composite specimens were prepared by hot pressing a stack of Ti–6Al–4V foils and monolayers of either uncoated boron, $B_4C$ coated boron or SiC CVD filaments (volume fraction $V_f = 0.32$). After annealing, the composite panels were electrodischarge machined. The single edge notch (SEN) specimen shape for crack propagation testing is shown in Fig. 1.

### 2.2. Heat treatments

Before notching, each specimen was heat treated at 850° C in vacuum for 9, 18, 36, 72 or 160 h. During these diffusion heat treatments, various interfacial reaction zones grow, depending upon the type of filament (and eventually the coating) and the thermal exposure duration.

The main features of the reaction zones are schematically illustrated in Fig. 2 and described in [2, 3].

From a mechanical standpoint, most phases built up at the FM interfaces are very brittle and generally characterized by rupture strains ($\varepsilon^R$) much smaller than those corresponding to the fibres (see Table I). The titanium silicides are the exception which might be meaningful with regard to the failure mechanisms of SiC/Ti–6Al–4V composites.

### 2.3. Testing procedure

Fatigue crack growth testing on the SEN specimens was performed in tension–tension using the following conditions:

(a) frequency of the sinusoidal loading cycles, 20 Hz,
(b) stress ratio, $R = 0.1$ ($R = \sigma_{min}/\sigma_{max}$),
(c) maximum stress, 130 to 150 MPa.

Crack lengths were measured by an optical method with the help of a cathetometer since the crack tip was easy to discern on the specimens.

From crack lengths ($a$) against number of cycles ($N$), the main features of crack propagation in the composites could be derived by means of:

(i) the determination of the crack growth rate $da/dN$ against the stress intensity factor range $\Delta K_I$ (using the secant method or a polynomial function fitting $a$–$N$ curves),

(ii) the assessment of the critical crack length $a_c$ corresponding to high rate crack propagation; $a_c$ values were derived from a polynomial extrapolation of the $a$–$N$ curves checked by optical examination of fracture surfaces (fracture surface appearances are different for progressive crack growth and sudden crack propagation leading to rupture).

It is noteworthy that several $a$–$N$ curves, related mostly to SiC/Ti–6Al–4V composites, could not be fitted by a polynomial $N = f(a^{1/2})$ corresponding to a $da/dN$–$\Delta K_I$ function similar to $da/dN = C\Delta K_I^m$

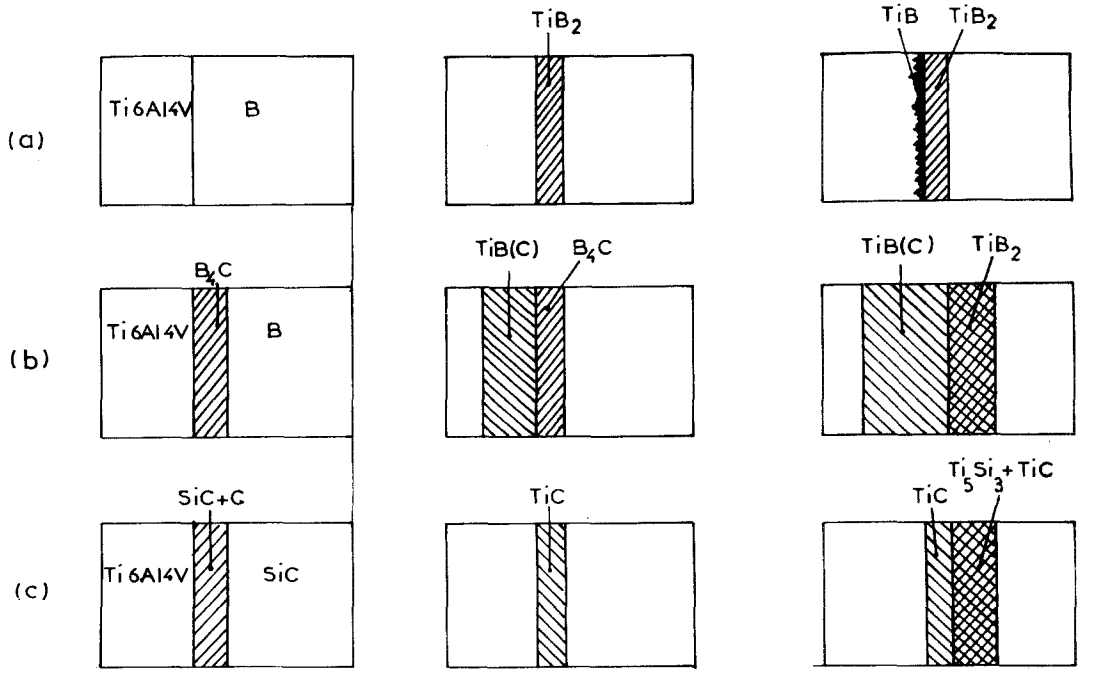


*Figure 2* Schematic illustration of the evolution of the main features of FM interfaces in titanium based composite materials (a) B/Ti–6Al–4V, (b) B($B_4C$)/Ti–6Al–4V and (c) SiC/Ti–6Al–4V.

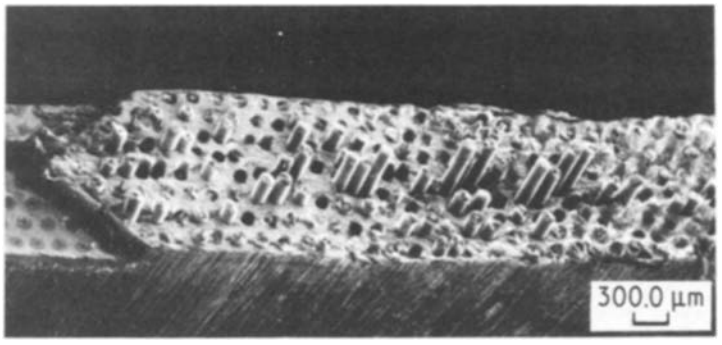


*Figure 3* SEM macrograph of surface failure in as-fabricated SiC/Ti–6Al–4V composite after fatigue crack growth.

where $C$ is a constant. In these cases the coefficient $m$ characterizing the crack growth acceleration when the stress intensity factor range increases could not be evaluated. However, most crack growth parameters were determined and averaged from the different procedures previously summarized and reported in detail by Quenisset *et al.* [1].

## 3. Crack growth features in as-fabricated B, B($B_4C$) and SiC/Ti–6Al–4V composites

### 3.1. Failure mode and crack growth curves

Crack extension was mainly coplanar with the notch for all the composite samples. This predominance of the opening mode I was enhanced by the relatively high stress level applied to the specimens during the tests (Fig. 3). However, crack extension in the direction parallel to the fibres could be observed on several SiC/Ti–6Al–4V specimens, though the final fracture surface in the titanium alloy matrix remains macroscopically regular and perpendicular to the fibres.

Typical $da/dN$–$\Delta K_I$ curves corresponding to specimens revealing no crack in the direction parallel to the fibres (mostly pure opening mode I) show quasi regular increase of $da/dN$ against $\Delta K_I$ as illustrated by the curve (a) in Fig. 4. On the other hand, the specimens which displayed crack extensions along the fibres corresponded to $da/dN$–$\Delta K_I$ curves similar to curve (b). Such curves are sometimes observed on SiC/Ti–6Al–4V composites in the as-fabricated condition or after a moderate heat treatment (9 h). The retarding effect due to delamination indicates somewhat of a notch insensitivity which renders difficult the assessment of the crack growth parameters $m$ and $\Delta K$ for $da/dN = 10^{-4}$ mm cycle$^{-1}$. Otherwise, comparison between curves (a) and (b) in Fig. 4 shows that the notch insensitivity features of curve (b) is not associated with a better toughness. It only indicates an effect of loading cycles on FM bonding. As the crack propagates, FM interfaces are weakened by fatigue, providing the material with better resistance to further crack growth even though $\Delta K_I$ increases.

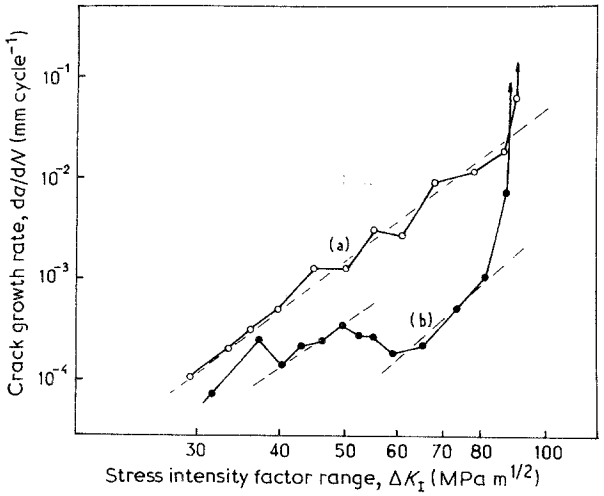


*Figure 4* Crack growth rate $da/dN$ against stress intensity factor range $\Delta K_I$ curve derived from the secant method, as-fabricated SiC/Ti–6Al–4V, $\sigma_{max} = 150$ MPa.

However, curves resulting from longitudinal crack growth and typified by curve (b) in Fig. 4 are sufficiently casual to consider that, for the stress level used, cracks propagate in the related composites according to the opening mode I of failure.

### 3.2. Crack propagation characteristics

Using $da/dN$–$\Delta K_I$ curves and the $a_c$ assessment, $\Delta K$ for $da/dN = 10^{-4}$ mm cycle$^{-1}$, $m$ and the apparent critical stress intensity factor $K_{I_{ac}}$ were evaluated for each specimen and are given in Table II (each entry being in general the average value of three and sometimes five or six tests).

A first examination of the results leads to the following remarks:

(a) The crack growth rates are the highest in the B/Ti–6Al–4V composites and remain smaller in B($B_4C$)/Ti–6Al–4V composites than in SiC/Ti–6Al–4V composites whatever the thermal exposure.

(b) The coefficients $m$ are similar for the three kinds of composite and remain small (about 4.5 in the as-fabricated conditions) despite the strong heterogeneity of the materials and particularly the mechanical mismatch between the matrix and the filaments.

(c) For the as-fabricated materials, the apparent critical stress intensity factors $K_{I_{ac}}$ are slightly higher than the matrix toughness (about 75 MPa m$^{1/2}$) when the reinforcement is either B($B_4C$) or SiC filaments (about 85 MPa m$^{1/2}$). In the case of B/Ti–6Al–4V composites, $K_{I_{ac}}$ values are very close to the matrix toughness itself.

(d) Several tests performed with relatively low stress levels (< 100 MPa) have shown that the fatigue threshold corresponding to mode I crack growth could be quite high in the composites compared to the Ti–6Al–4V alloy. It is particularly the case for SiC/Ti–6Al–4V composites for which cracks do not grow in other directions than that of the fibre when $\Delta K_I < 20$ MPa m$^{1/2}$.

### 3.3. Damage mechanism

As previously reported [1] for B/Ti–6Al–4V composites, optical examination of the fibres in the vicinity

TABLE II Crack growth parameters

| MMC | Isothermal exposure at 850° C (h) | Number of tests | $m$ | $\Delta K_I$ (MPa m$^{1/2}$) for $da/dN = 10^{-4}$ mm cycle$^{-1}$ | $K_{I_{ac}}$ (MPa m$^{1/2}$) |
|---|---|---|---|---|---|
| B/Ti–6Al–4V | 0 | 6 | $4.3 \pm 0.3$ | $26 \pm 2$ | $74 \pm 3$ |
| | 7 | 3 | $4.1 \pm 0.2$ | $28 \pm 2$ | $79 \pm 2$ |
| | 9 | 4 | $4 \begin{smallmatrix}+0.4\\-0.2\end{smallmatrix}$ | $27 \pm 3$ | $82 \begin{smallmatrix}+3\\-5\end{smallmatrix}$ |
| | 18 | 4 | $4.2 \begin{smallmatrix}+0.2\\-0.3\end{smallmatrix}$ | $25 \begin{smallmatrix}+4\\-3\end{smallmatrix}$ | $79 \pm 5$ |
| | 36 | 4 | $4.6 \begin{smallmatrix}+0.1\\-0.3\end{smallmatrix}$ | $24 \begin{smallmatrix}+2\\-3\end{smallmatrix}$ | $77 \begin{smallmatrix}+4\\-6\end{smallmatrix}$ |
| | 72 | 3 | $5.3 \pm 0.2$ | $23 \pm 2$ | $64 \begin{smallmatrix}+3\\-4\end{smallmatrix}$ |
| | 160 | 1 | 6 | 18 | 44 |
| B($B_4C$)/Ti–6Al–4V | 0 | 3 | $4.6 \pm 0.3$ | $39 \begin{smallmatrix}+2\\-3\end{smallmatrix}$ | $84 \pm 3$ |
| | 9 | 3 | $4.6 \pm 0.2$ | $37 \begin{smallmatrix}+3\\-2\end{smallmatrix}$ | $87 \begin{smallmatrix}+6\\-5\end{smallmatrix}$ |
| | 18 | 3 | $4.7 \begin{smallmatrix}+0.3\\-0.2\end{smallmatrix}$ | $36 \pm 2$ | $88 \pm 3$ |
| | 36 | 2 | $4.9 \pm 0.3$ | $34 \pm 2$ | $88 \pm 5$ |
| | 72 | 3 | $5.4 \begin{smallmatrix}+0.4\\-0.3\end{smallmatrix}$ | $31 \begin{smallmatrix}+2\\-1\end{smallmatrix}$ | $81 \begin{smallmatrix}+5\\-4\end{smallmatrix}$ |
| | 160 | 3 | $5.9 \begin{smallmatrix}+0.4\\-0.3\end{smallmatrix}$ | $26 \begin{smallmatrix}+2\\-3\end{smallmatrix}$ | $56 \pm 5$ |
| SiC/Ti–6Al–4V | 0 | 5 | $4.5 \begin{smallmatrix}+0.4\\-0.5\end{smallmatrix}$ | $33 \pm 3$ | $87 \pm 4$ |
| | 9 | 4 | $4.9 \begin{smallmatrix}+0.2\\-0.1\end{smallmatrix}$ | $30 \pm 4$ | $79 \pm 3$ |
| | 18 | 4 | $4.9 \pm 3$ | $27 \begin{smallmatrix}+3\\-2\end{smallmatrix}$ | $80 \pm 5$ |
| | 36 | 1 | 5.3 | 30 | 87 |
| | 72 | 4 | $5.8 \begin{smallmatrix}+0.3\\-0.2\end{smallmatrix}$ | $31 \begin{smallmatrix}+2\\-3\end{smallmatrix}$ | $90 \begin{smallmatrix}+5\\-6\end{smallmatrix}$ |
| | 160 | 1 | 6.1 | 25 | 70 |

of the crack tip reveals, in as-fabricated B($B_4C$)/Ti–6Al–4V composites, a damage mechanism allowing plastic deformation by means of fibres microcracking.

On the other hand, no such damage zone (also called splitting zone) can be seen on each side of cracks in the as-fabricated SiC/Ti–6Al–4V composites or after moderate heat treatments (9 h). This feature, illustrated in Fig. 5, points out an apparent contradiction since the absence of the splitting mechanism (associated with energy dissipation) does not lead to lower toughness.

In order to explain the above observation and then the influence of fatigue and thermal exposure on crack growth and failure mechanisms, the conditions for which a damage zone occurs will be defined through the schematic representation in Fig. 6. Consider $r_f$ the characteristic size of the strain concentration field in the vicinity of the macrocrack tip. $2r_f$ is the width of the area within which the strain in the fibres ($\varepsilon_f$) is higher than the fibre rupture strain ($\varepsilon_f^R$). The length necessary to ensure load transfer from fibres to matrix ($l_c$) is generally considered roughly equal to the distance between fibre breaks ($L$). Thus; two cases must be discussed:

(a) If $2r_f < l_c$, only one break occurs in each fibre, there is no damage zone.

(b) If $2r_f > l_c$, each fibre can be divided into several short fibres, leading to the build up of a damage zone.

As a result the number of failures in each fibre ($N$) leading to energy dissipation in the matrix depends on:

(i) the strain concentration field (that is $\Delta K_I$). Indeed, the damage zones have always been found smaller in the specimens zones failed by fatigue than in overload zones.

(ii) The fibre rupture strain $\varepsilon_f^R$. A particularly high rupture strain (as for SiC fibres before degradation) may prevent any damage zone build up.

(iii) The FM bonding characterized by $l_c$ is given by the following formula:

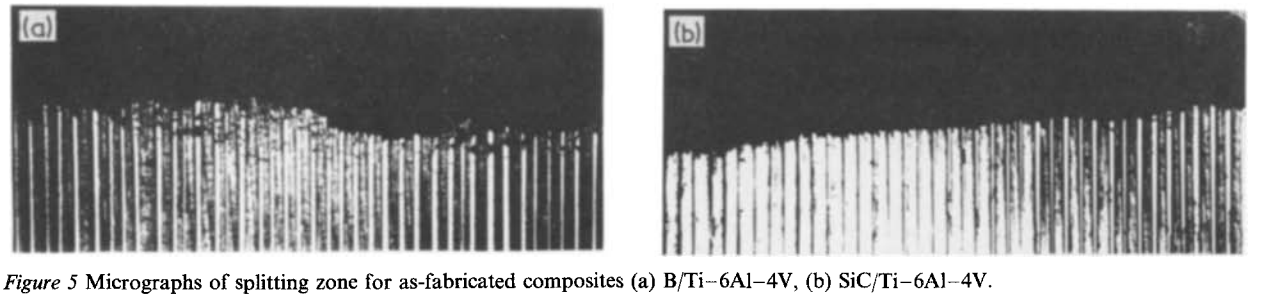


*Figure 5* Micrographs of splitting zone for as-fabricated composites (a) B/Ti–6Al–4V, (b) SiC/Ti–6Al–4V.

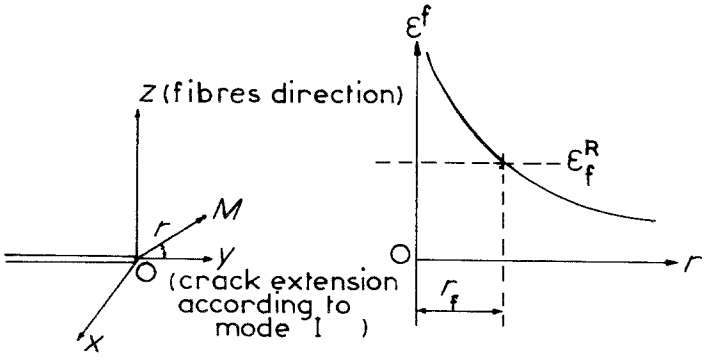


*Figure 6* Schematic representation of strain concentration field around a crack tip in MMC.

$$l_c = \frac{\varepsilon_f^R E_f d}{\tau_i} \quad (1)$$

where $d$ is the fibre diameter, $E_f$ the Young's modulus of the fibre and $\tau_i$ the FM interfacial shear strength.

An analysis of the effect of thermal exposure on the composite characteristics will provide a basis for further discussion of failure mechanisms.

## 4. Effect of isothermal exposure

### 4.1. Effect of diffusion heat treatment on crack growth characteristics

The evolution of the crack growth parameters against the isothermal exposure duration is illustrated in Figs. 7 to 11. From these figures the following conclusions can be drawn:

(a) The increase in microhardness of the Ti–6Al–4V matrix occurring during the diffusion heat treatment is about the same for all types of composites (Fig. 7).

(b) Damage zones are already present in as-fabricated B/Ti–6Al–4V and B($B_4C$)/Ti–6Al–4V test specimens, but they appear only after a short duration heat treatment (10 h) in the case of SiC/Ti–6Al–4V composites. In all cases, they grow with the diffusion treatment duration up to a critical thermal exposure time which depends on the type of composite. For further thermal exposure they become smaller and finally disappear (Fig. 8).

(c) The main effect of thermal exposures on the crack growth rate is a raising effect ($\Delta K_I$ decreases for a given growth rate) though $\Delta K_I$ for $da/dN = 10^{-4}$ mm cycle$^{-1}$ increases somewhat after short heat treatments in the case at B/Ti–6Al–4V composites (Fig. 9). The lowest crack growth rate is obtained for B($B_4C$)/Ti–6Al–4V composites.

(d) After short heat treatments (< 10 h) the crack growth exponents $m$ related to boron and $B_4C$ reinforced matrices respectively decreased or remained constant. On the contrary $m$ increased in the case of SiC/Ti–6Al–4V composites. This discrepancy between the effects of heat treatments on the three types of materials disappears for further thermal exposures ($m$ rising with time in any case) (Fig. 10).

(e) Deviations in toughness evolution are also illustrated (Fig. 11). The apparent discrepancy between the effects of isothermal exposure on toughness on the three types of composites is not so significant if we consider that the toughness evolution includes the following three stages.

A first stage, corresponding to short diffusion heat treatments, during which toughness decrease, as can be observed in the case of SiC/Ti–6Al–4V. For both boron and B($B_4C$) reinforced materials this stage might be included in the composite processing. During the second stage, corresponding to longer thermal exposures, toughness is increased. Finally, the third stage corresponds to further heat treatments and progressive degradation of the crack growth characteristics of the composites.

### 4.2. Fracture surfaces

In general, the fracture surfaces of the three types of composites do not exhibit evidence of the pull-out phenomenon, as already reported for B/Ti–6Al–4V composites, though a small amount of pull-out can be observed in the as-fabricated materials [1]. The effect of load cycling seems also to be quite similar for boron, B($C_4C$) and SiC reinforced matrices: the

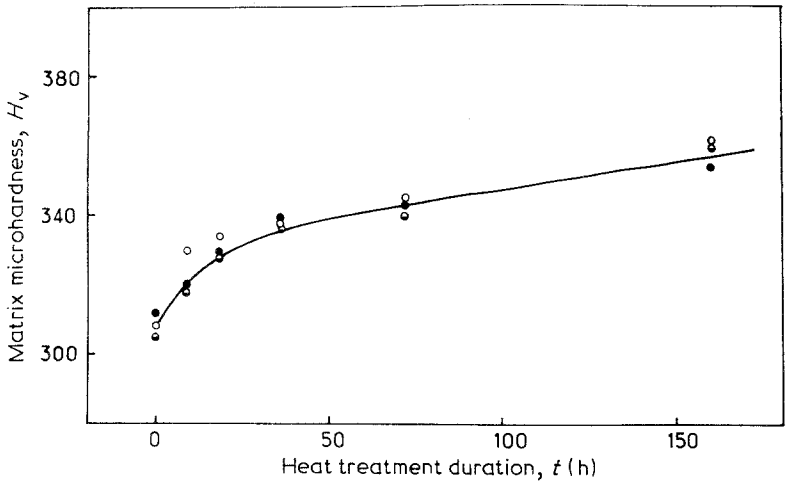


*Figure 7* Effect of thermal exposure on matrix microhardness. $V_f = 0.32$, (◑) B/Ti–6Al–4V, (○) B($B_4C$)/Ti–6Al–4V, (●) SiC/Ti–6Al–4V, testing load: 200 g.

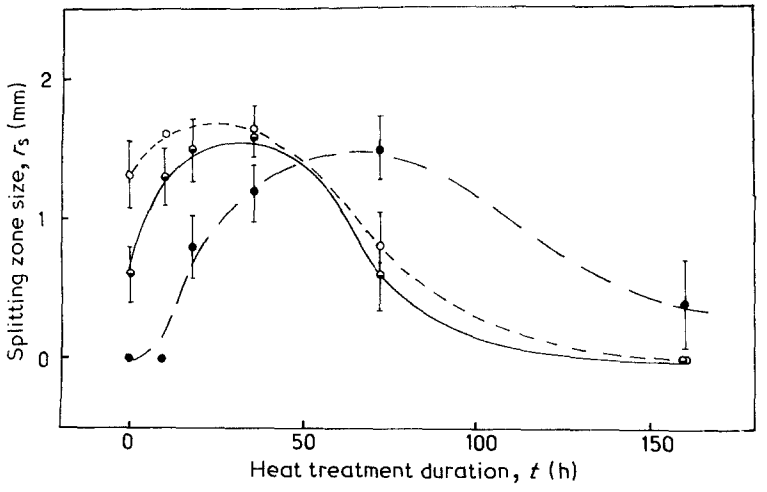


*Figure 8* Effect of thermal exposure on the damage zone size measured on the first filament layer of the specimen. $V_f = 0.32$, (◑) B/Ti–6Al–4V, (○) B($B_4C$)/Ti–6Al–4V, (●) SiC/Ti–6Al–4V.

fatigue zone of the matrix is obvious, as shown in Fig. 12, and the damage zone is reduced due to crack propagation with smaller $\Delta K_I$, as previously explained. Other features of rupture surfaces are identical for the three types of composites, such as:

(a) intermittent crack growth in mode II showing the impeding effect of the fibres,

(b) small debonding effect between reaction zone and matrix for short thermal exposures,

(c) significant debonding between fibres and reaction zones for long thermal exposures associated with an extensive degradation of the reinforcement,

(d) numerous microcracks appearing in the FM interfaces and leading to crack initiation in the fibres and the matrix when the reaction zone is thick enough to activate a notch effect.

However, in as-fabricated conditions and for moderate thermal exposures SiC/Ti–6Al–4V composites do not exhibit microcracking in the reaction zone as do the boron and B($B_4C$) reinforced matrices (Fig. 13).

### 4.3. Crack growth and rupture mechanisms

Since few pull out phenomena were observed in boron, B($B_4C$) and SiC/Ti–6Al–4V composites and since the reinforcements are very brittle materials, fracture energy is mostly due to: (a) matrix failure work, mainly the energy of plastic deformation (*Um*), (b) elastic strain energy released at fibre breaks and transferred from fibre to matrix (*Ut*).

*Um* can be assessed from the toughness of Ti–6Al–4V and *Ut* can be derived from the following approximate formula [9]:

$$Ut \sim \varepsilon_f^{R^2} L V_f N E_f \qquad (2)$$

Correlation between crack growth data, damage zone analysis, fracture surface examination and rupture work evaluation suggest the following crack growth and rupture mechanisms (Fig. 14).

1. In as-fabricated composites the FM debonding effect occurring during crack growth and the high rupture strain of the fibres (not yet degraded by heat treatment) give rise to high fibre critical length. Therefore, $L$ is not small compared to $2r_f$ and damage zones are small in extent. This effect is particularly significant in SiC/Ti–6Al–4V composites for which the FM interface is more smooth, allowing easier FM sliding than in the case of B/Ti–6Al–4V and B($B_4C$)/Ti–6Al–4V composites (Fig. 13). Thus the damage zone is expected to be almost non existent in as-fabricated SiC/Ti–6Al–4V composites as effectively observed (Fig. 14a). Nevertheless, failure work can remain high as shown by Equation 2.

2. When the composites are weakly heat treated, the various parameters of *Ut* change as follows:

(a) $\varepsilon_f^R$ decreases due to fibre degradation and notch

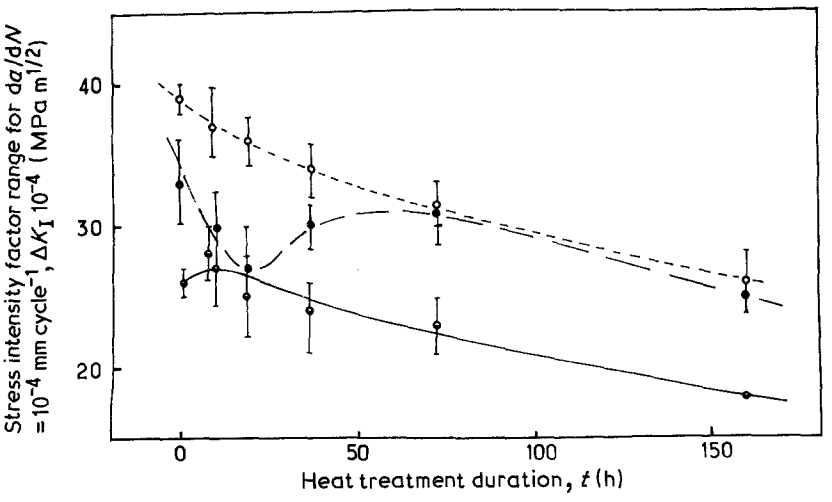


*Figure 9* Effect of thermal exposure on crack growth rate. $V_f = 0.32$, (◑) B/Ti–6Al–4V, (○) B($B_4C$)/Ti–6Al–4V, (●) SiC/Ti–6Al–4V.

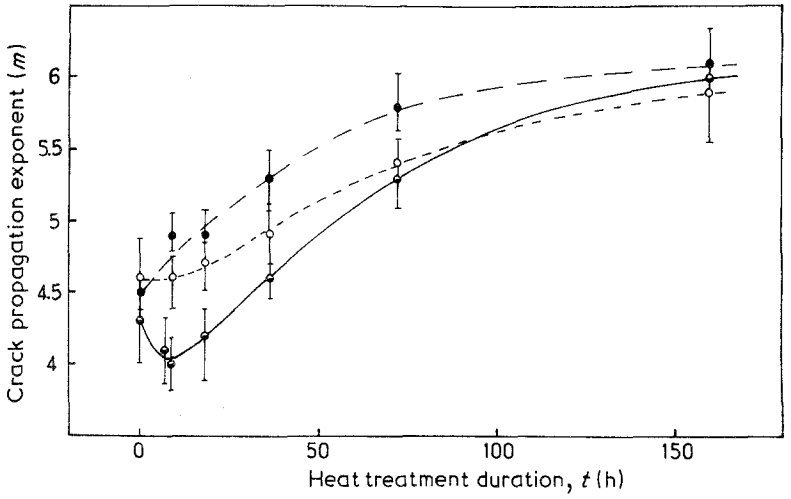


*Figure 10* Effect of thermal exposure on crack propagation exponent. $V_f = 0.32$, (◑) B/Ti–6Al–4V, (○) B($B_4C$)/Ti–6Al–4V, (●) SiC/Ti–6Al–4V.

effects related to the microcracks built up in the growing reaction zones;

(b) therefore $r_f$ increases. This increase is related to the number of fibre breaks since their failure lowers locally the Young's modulus of the composite and results in a more widely spread strain concentration field;

(c) simultaneously FM bonding increases, resulting in a diminution of the fibre critical length;

(d) there results a strong increase in the number of fibre failures if $2r_f > L$.

Depending on $r_f$ compared to $L$ thermal exposure leads to opposite tendencies in the evolution of $Ut$:

(i) As long as $2r_f < L$, only one break occurs in each fibre and the lack of damage zone prevents the decrease in $\varepsilon_f^R$ and $L$ to be compensated by an increase in $N$. That is the case of SiC/Ti–6Al–4V composites for short thermal exposures (up to about 10 h). The corresponding decrease in toughness is stronger as matrix microhardness increases (Fig. 14b).

(ii) As soon as $2r_f > L$, an increase in $N$ gives rise to larger and larger damage zones so that $Ut$ increases, as well as the composite toughness, despite the decrease in matrix ductility. Boron, B($B_4C$) and SiC/Ti–6Al–4V exhibit such an evolution with thermal exposure duration (up to 10 h for B/Ti–6Al–4V, 30 h for B($B_4C$)/Ti–6Al–4V and about 60 h for SiC/Ti–6Al–4V, see Fig. 14c). The delayed evolution in crack growth parameters for the SiC/Ti–6Al–4V composites compared to boron and B($B_4C$)/Ti–6Al–4V composites when the thermal exposure duration increases, could be partly attributed to the differences in morphology, rigidity and rupture strain between the various reaction zone phases.

3. After long heat treatments, $\varepsilon_f^R$ no longer decreases. In fact, $\varepsilon_f^R$ is equal to the rupture strain of the interfacial phases since the reaction zone is so thick that failure of the fibre and reaction zone occurs simultaneously [10]. Nevertheless, the damage zone disappears progressively due to the extensive degradation of the fibre–reaction zone bonding so that $L$ decreases as well as $N$. Indeed, debonding is observed between fibres and reaction zones for composites heat treated for 160 h, as illustrated in Fig. 15. However, no significant pull out phenomenon has been observed since the crack joins with reaction zone microcracks which initiate fibre failure. The resulting fracture surfaces are particularly rough and the only damaging mechanism remaining is related to reaction zone microcracking. The microcracks induce some energy dissipation by elastic strain release in the matrix though increases in microcrack spacing (see Figs. 13 and 15).

It is noteworthy that crack growth rates ($\Delta K_I$ for $da/dN = 10^{-4}$ mm cycle$^{-1}$) and the exponent $m$, mainly agree with the change of $K_{I_{ac}}$ with duration of isothermal exposure. This suggests that crack growth mechanisms are similar during fatigue crack propagation and overload failure. However crack growth investigations in the specimen zone failed by fatigue

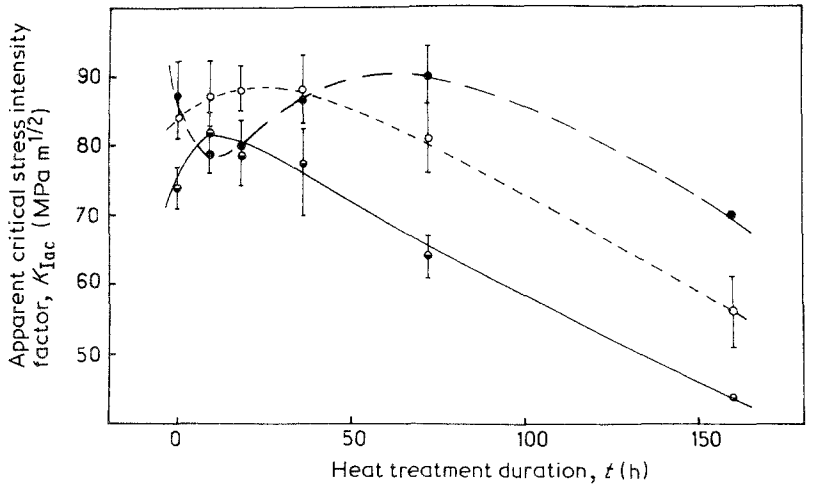


*Figure 11* Effect of thermal exposure on toughness. $V_f = 0.32$, (◑) B/Ti–6Al–4V, (○) B($B_4C$)/Ti–6Al–4V, (●) SiC/Ti–6Al–4V.

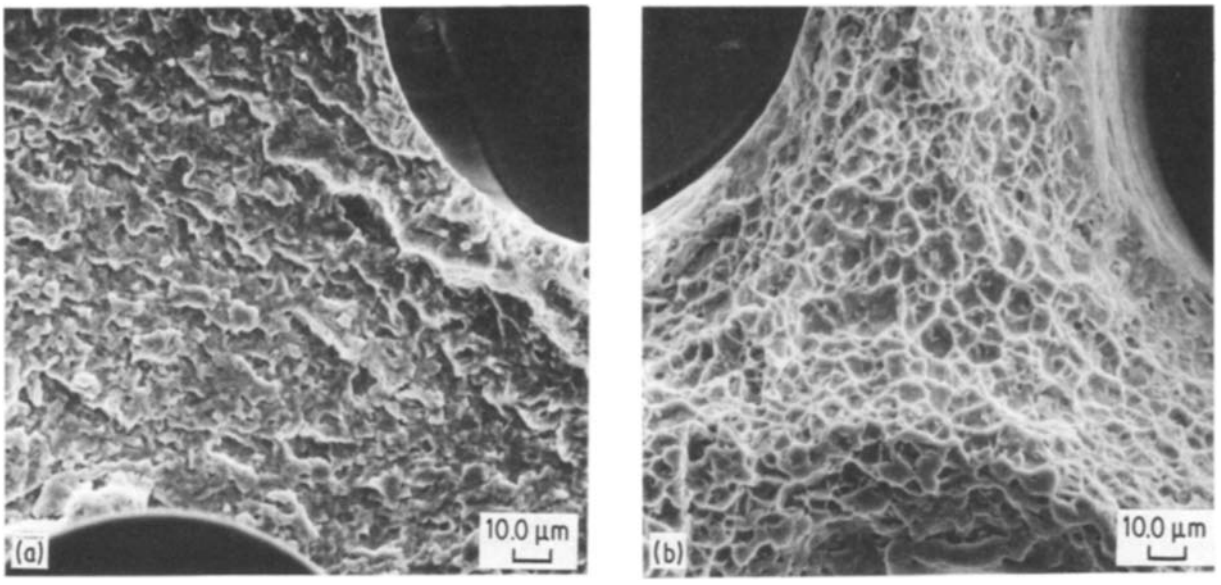


*Figure 12* SEM micrographs of matrix failure surfaces in SiC/Ti–6Al–4V composites, (a) fatigue zone, (b) overload zone.

emphasize different features of rupture mechanisms. For example, as shown in Fig. 13, fatigue better points out differences between reaction zone behaviours in $B(B_4C)$ and SiC/Ti–6Al–4V composites than does overloading.

## 5. Conclusions

Using crack propagation testing, comparison between the failure mechanisms in boron, $B(B_4C)$ and SiC reinforced Ti–6Al–4V composites first emphasizes the favourable retarding effect of the fibres on the crack growth parameters of the three types of composites with respect to the Ti–6Al–4V alloy.

The parameters measured are the crack growth rate ($\Delta K_I$ for $da/dN = 10^{-4}$ mm cycle$^{-1}$), the crack growth exponent $m$ and the apparent critical stress intensity factor $K_{I_{ac}}$ (presently considered as toughness).

The change of these parameters and the main features of fracture surfaces as the composites are heat treated lead to distinguish boron and $B(B_4C)$/Ti–6Al–4V composites on the one hand and SiC/Ti–6Al–4V composites on the other:

(a) In the first case, a short isothermal exposure at 850° C improves crack growth behaviour. $K_{I_{ac}}$ increases, $m$ decreases or remains constant and $\Delta K_I$ for $da/dN = 10^{-4}$ increases except for $B(B_4C)$/Ti–6Al–4V composites. This improvement is attributed to microcracks in the fibres and the reaction zone in the vicinity of the crack tip, giving rise to a damaging mechanism. Further heat treatments lead to complete degradation of the composites and therefore the crack growth resistance decreases.

(b) In the second case, a short thermal exposure strongly decreases the crack growth resistance, mainly due to fibre strength decrease, matrix hardness increase and improvement of the fibre matrix bonding when the damaging mechanism is not yet possible. However, after about 10 h of thermal exposure, the effect of heat treatment on crack growth mechanisms and parameters is identical for the three types of com-

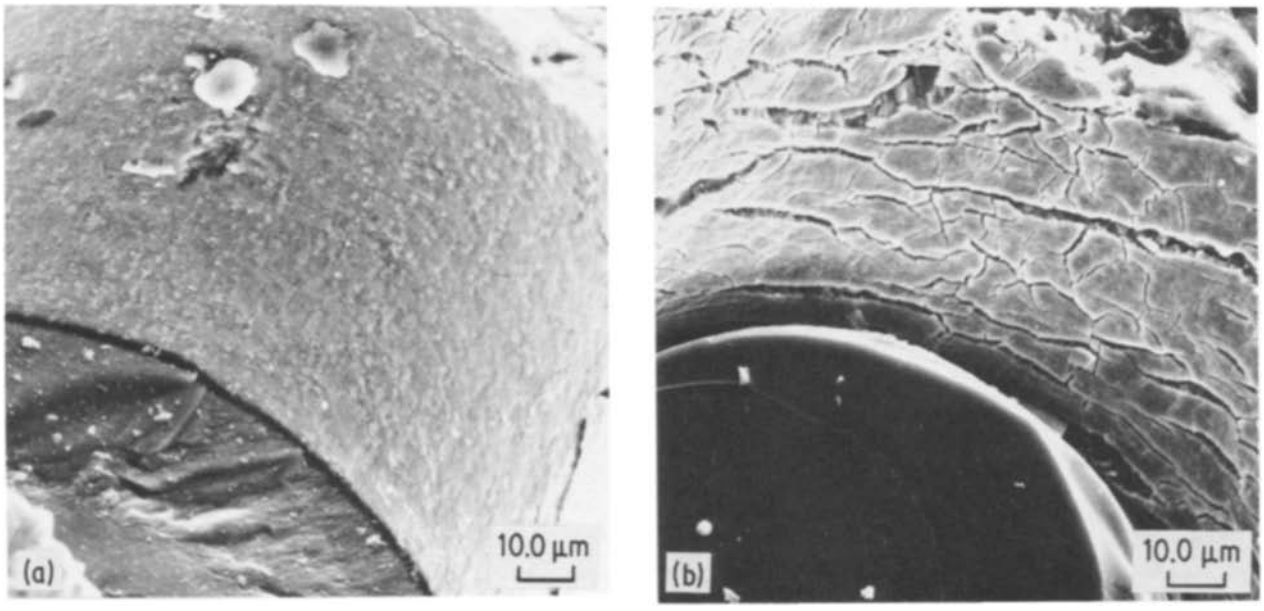


*Figure 13* SEM micrographs of the FM reaction zone in as-fabricated composites (fatigue zone) (a) SiC/Ti–6Al–4V, (b) $B(B_4C)$/Ti–6Al–4V.

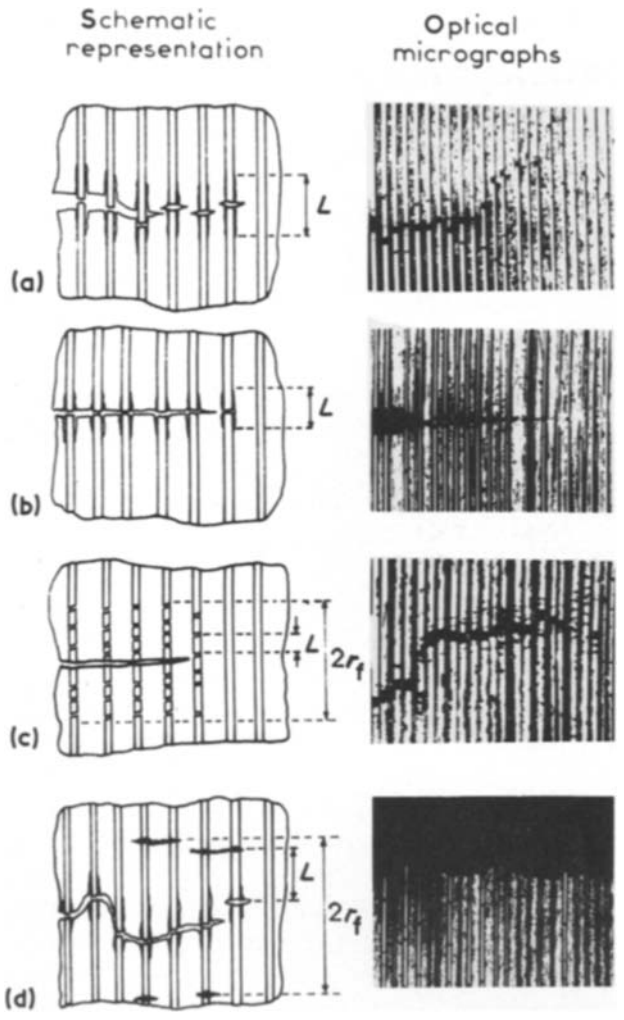


*Figure 14* Schematic representation of crack growth mechanism against isothermal exposure in titanium based composites. SiC/Ti–6Al–4V, (a) as-fabricated, (b) 9 h at 850° C, (c) 36 h at 850° C. (d) $B(B_4C)$/Ti–6Al–4V, 160 h at 850° C.

posites. The influence of isothermal exposure on crack growth behaviour seems to be delayed for SiC/Ti–6Al–4V compared to boron and $B(B_4C)$/Ti–6Al–4V composites. The retarding effect has not been attributed to a lower reactivity of SiC fibres but rather to morphology, rigidity and rupture strain differences between the reaction zone phases.

Depending on the stress intensity factor at the crack tip, the fatigue load cycling does not change the crack growth mechanisms but better contrasts their different features.

## Acknowledgements

The authors wish to thank Siemens Company for electrodischarged machining of the specimens as well as R. Pailler and P. Martineau for preparation of composite foils.

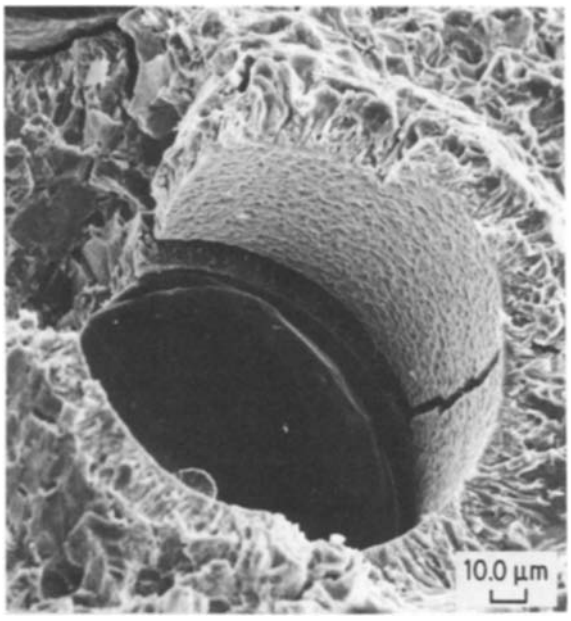


*Figure 15* SEM micrograph of fracture surface in $B(B_4C)$/Ti–6Al–4V composite after a long heat treatment (160 h, 850° C).

## References

1. J. M. QUENISSET, P. SOUMELIDIS, R. PAILLER, R. NASLAIN and N. S. STOLOFF, *J. Mater. Sci.* (to be published).
2. R. NASLAIN, J. THEBAULT and R. PAILLER, Proceedings of the International Conference on Composite Materials, Geneva and Boston, April 1975, edited by E. Scala, E. Anderson, I. Toth and B. R. Noton (TMS-AIME, New York, 1975) p. 116.
3. P. MARTINEAU, R. PAILLER, M. LAHAYE and R. NASLAIN, *J. Mater. Sci.* **19** (1984) 2749.
4. J. L. PENTECOST, "High Temperature Inorganic Coatings" edited by J. Huminik (1963) pp. 10–45.
5. J. H. WESTBROOK and E. R. STOWER, in "High Temperature Materials and Technology", edited by Campbell and Sherwood (J. Wiley, New York, 1967) pp. 312–48.
6. I. E. CAMPBELL, C. F. POWEL, D. H. NOWICK and B. W. GONSER, *J. Electrochem. Soc.* **96**(5) (1949) 318.
7. G. V. SAMSONOV and A. P. EPIK, "Coating of High Temperature Materials", (Plenum Press, New York, 1966) pp. 97–106.
8. E. RUDY, Technical report AFML-TR. 65-2, Part. V, (1969).
9. M. PIGOTT, *J. Mater. Sci.* **5** (1970) 669.
10. A. J. METCALE and M. J. KLEIN, in "Composite Materials", Vol. 1, Ch. 4, (Academic Press, New York, London, 1974) pp. 125–8.
11. F. W. CROSSMAN and A. S. YUE, *Met. Trans.* **2** (1971) 1545.

*Received 29 March*
*and accepted 21 May 1985*